

# **Plasmon-induced Electron Injection into the Large Negative Potential Conduction Band of Ga<sub>2</sub>O<sub>3</sub> for Coupling with Water Oxidation**

Yaguang Wang,<sup>a</sup> Xu Shi,<sup>a</sup> Tomoya Oshikiri,<sup>a</sup> Shuai Zu,<sup>a</sup> Kosei Ueno<sup>b</sup> and Hiroaki Misawa<sup>a,c\*</sup>

a. Research Institute for Electronic Science, Hokkaido University, Sapporo, Japan.

b. Department of Chemistry, Faculty of Science, Hokkaido University, Sapporo, Japan.

c. Center for Emergent Functional Matter Science, National Chiao Tung University, Hsinchu, Taiwan.

Correspondence and requests for materials should be addressed to H. Misawa (\*misawa@es.hokudai.ac.jp)

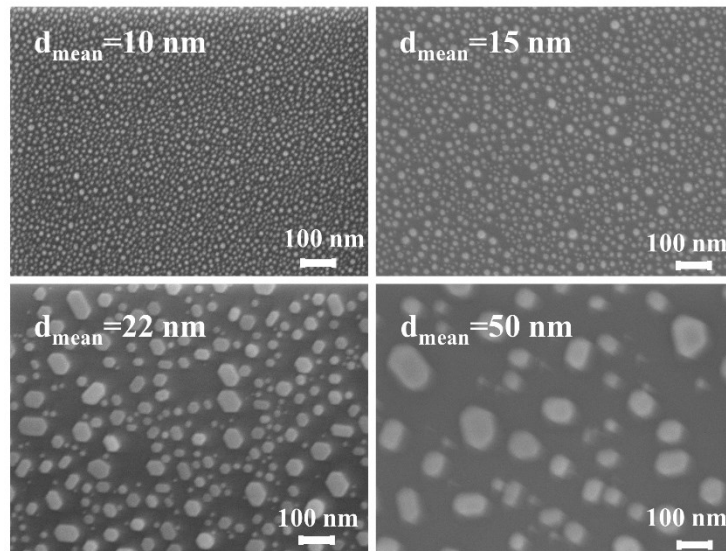


**Fig. S1** Top-view SEM images showing surface morphology of samples fabricated by annealing Au film with different thickness.

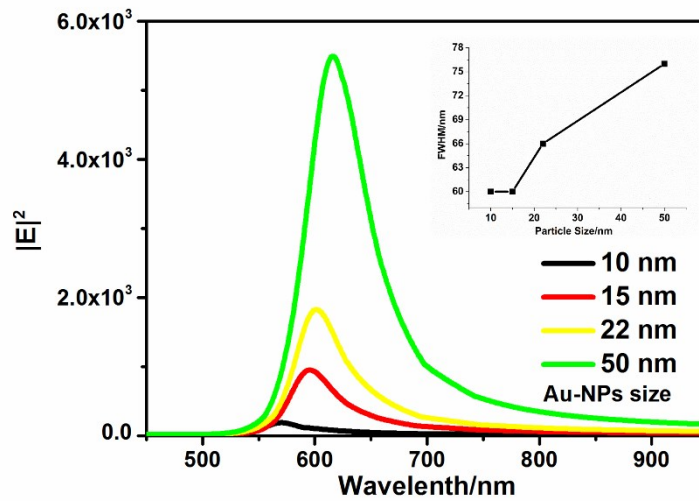


**Fig. S2** Near-field spectra on Au-NPs/Ga<sub>2</sub>O<sub>3</sub> interface with different Au-NPs size simulated by the FDTD method. Inset: FWHMs of the spectra.

In Fig. S2, full-field electromagnetic wave simulations were performed using the finite-difference time-domain method solver (FDTD Solutions, Lumerical). The ellipsoid sphere with various diameters of 10 nm, 15 nm, 22 nm and 50 nm in the x and y directions were used to model the Au-NPs. Accordingly, the z direction was set as 7 nm, 10 nm, 13 nm and 24 nm. The investigated structure was simulated using perfectly matched layers along z-direction and periodic boundary conditions along x-and y-directions with period of 15, 20, 35 and 80 nm, respectively. In the simulation, the refractive index was taken from the optical constants of Johnson and Christy. Ga<sub>2</sub>O<sub>3</sub> was treated as dielectric materials with refractive index of 1.8.

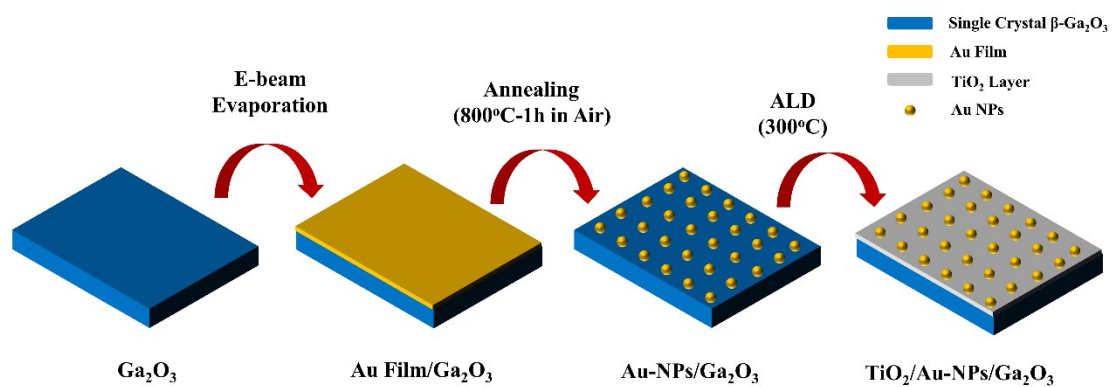


**Fig. S3** Schematics of the fabrication procedure for the TiO<sub>2</sub>/Au-NPs/Ga<sub>2</sub>O<sub>3</sub> photoelectrode.

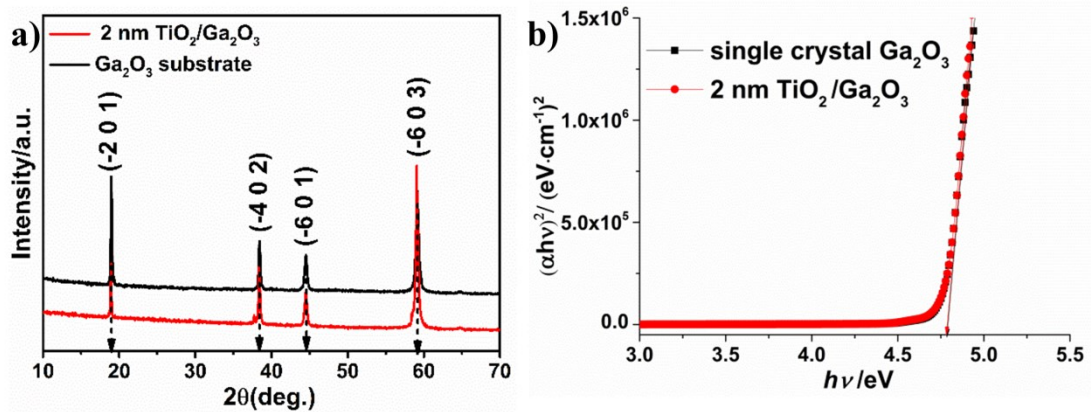


**Fig. S4** (a) XRD of single crystal  $\text{Ga}_2\text{O}_3$  with and without  $\text{TiO}_2$  (2 nm). (b) Tauc plots of single crystal  $\text{Ga}_2\text{O}_3$  with and without  $\text{TiO}_2$  (2 nm) calculated from the UV-Vis spectra.

All the peaks in XRD are attributed to the diffraction peaks of  $\beta\text{-Ga}_2\text{O}_3$ . No peaks shift and broadening of  $\text{Ga}_2\text{O}_3$  were observed after the deposition of  $\text{TiO}_2$ . Figure S4b shows the profile of  $(\alpha h\nu)^2$  versus  $h\nu$  for the single crystal  $\text{Ga}_2\text{O}_3$  with and without  $\text{TiO}_2$  (2 nm) which is related to the equation:

$$\alpha h\nu = A(h\nu - E_g)^n$$

where  $A$  is a constant,  $n=1/2$  for direct band gap semiconductor,  $\alpha$  is the absorption coefficient,  $h$  is the Planck constant,  $\nu$  is the light frequency. The bandgap energies ( $E_g$ ) were estimated from the x-intercept of Fig. S4b.

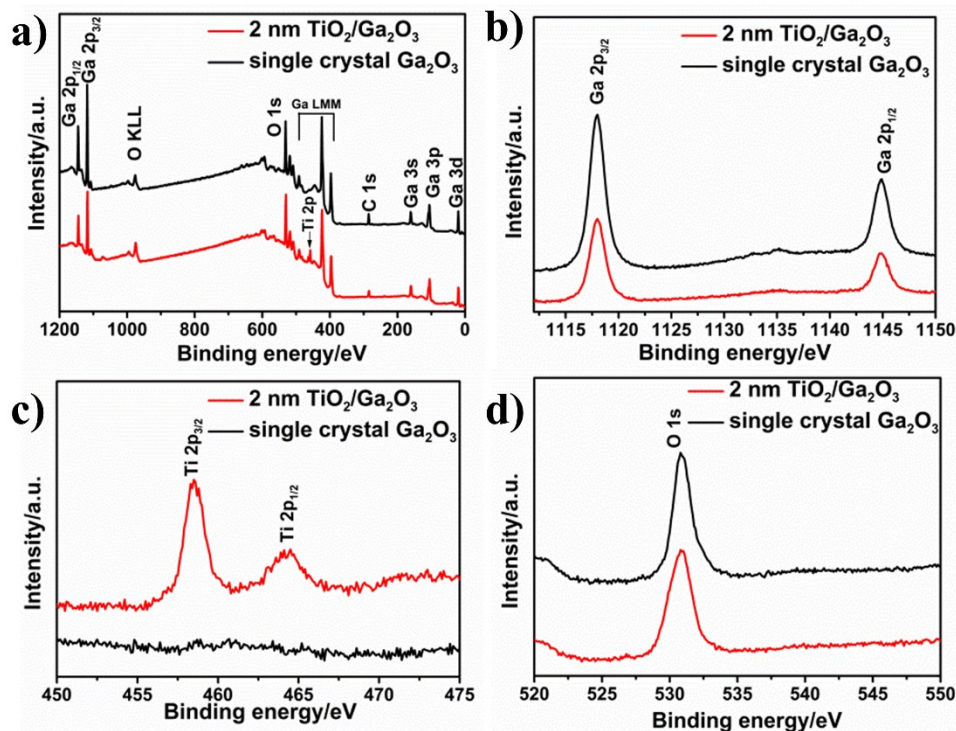


**Fig. S5** XPS spectra of single crystal Ga<sub>2</sub>O<sub>3</sub> with and without TiO<sub>2</sub> (2 nm): (a) full survey spectra; (b) core level spectra for Ga 2p; (c) core level spectra for Ti 2p; (d) core level spectra for O 1s.

Two symmetrical peaks of Ga 2p<sub>1/2</sub> (1144.5 eV) and Ga 2p<sub>3/2</sub> (1117.9 eV) were attributed to the Ga<sup>3+</sup> in Ga<sub>2</sub>O<sub>3</sub>.<sup>1</sup> After the deposition of TiO<sub>2</sub>, peaks of Ti 2p<sub>3/2</sub> and Ti 2p<sub>1/2</sub> at binding energies of 458.6 eV and 464.4 eV appeared indicating the presence of Ti<sup>4+</sup> in TiO<sub>2</sub>. The binding energy of O 1s peak of Ga<sub>2</sub>O<sub>3</sub> was observed at 530.7 eV. After TiO<sub>2</sub> deposition, the binding energy of O 1s peak shows slightly broadening at the lower energy side rather than peak energy shift, which is ascribed to the presence of O 1s peak of Ti-O (529.8 eV).<sup>2</sup>

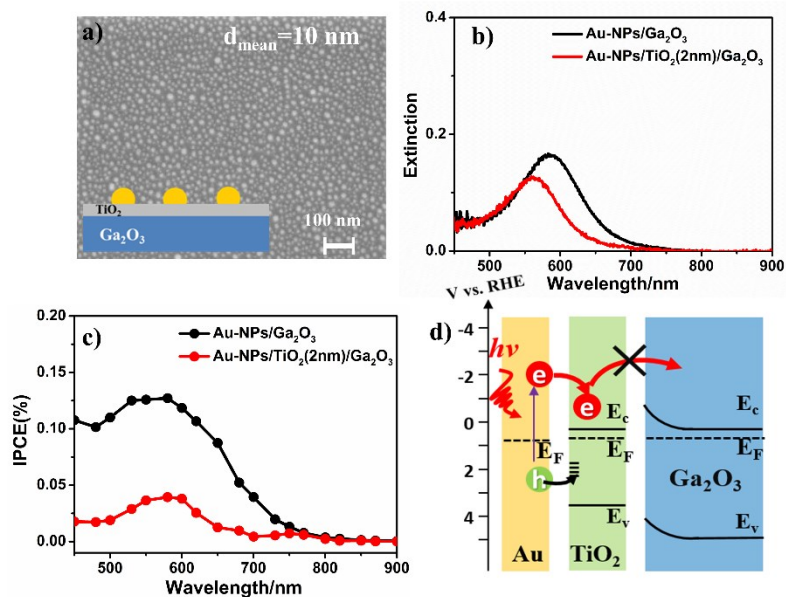


**Fig. S6** (a) The top-view SEM image of Au-NPs/TiO<sub>2</sub> (2 nm)/Ga<sub>2</sub>O<sub>3</sub>. Inset: schematic of Au-NPs/TiO<sub>2</sub>/Ga<sub>2</sub>O<sub>3</sub> structure. (b) Extinction spectra and (c) IPCE action spectra of Au-NPs/Ga<sub>2</sub>O<sub>3</sub> and Au-NPs/TiO<sub>2</sub> (2 nm)/Ga<sub>2</sub>O<sub>3</sub>. (d) Schematic diagram of charges transfer in Au-NPs/TiO<sub>2</sub>/Ga<sub>2</sub>O<sub>3</sub>.

TiO<sub>2</sub> is deposited on the surface of Ga<sub>2</sub>O<sub>3</sub> before the annealing process as shown in the inset in Fig. S6a (Au-NPs/TiO<sub>2</sub>/Ga<sub>2</sub>O<sub>3</sub>). Au-NPs/TiO<sub>2</sub>/Ga<sub>2</sub>O<sub>3</sub> had a blue shift of LSPR peak and weaker LSPR intensity compared with Au-NPs/Ga<sub>2</sub>O<sub>3</sub> as shown in Fig. S6b due to the smaller particle size of Au-NPs ( $d_{\text{mean}} \sim 10$  nm). However, the application of the TiO<sub>2</sub> layer between Au-NPs and Ga<sub>2</sub>O<sub>3</sub> dramatically decreases the IPCE to one-third of the value without TiO<sub>2</sub> as shown in Fig. S6c. The hot electrons generated by the photoirradiation would first be transferred to the TiO<sub>2</sub> layer adjacent to Au-NP. The electron transfer from CB of TiO<sub>2</sub> to the more negative CB of Ga<sub>2</sub>O<sub>3</sub> is difficult as shown in Fig. S6d. This unfavorable electron transfer process and weaker LSPR effect lead to the IPCE decrease.

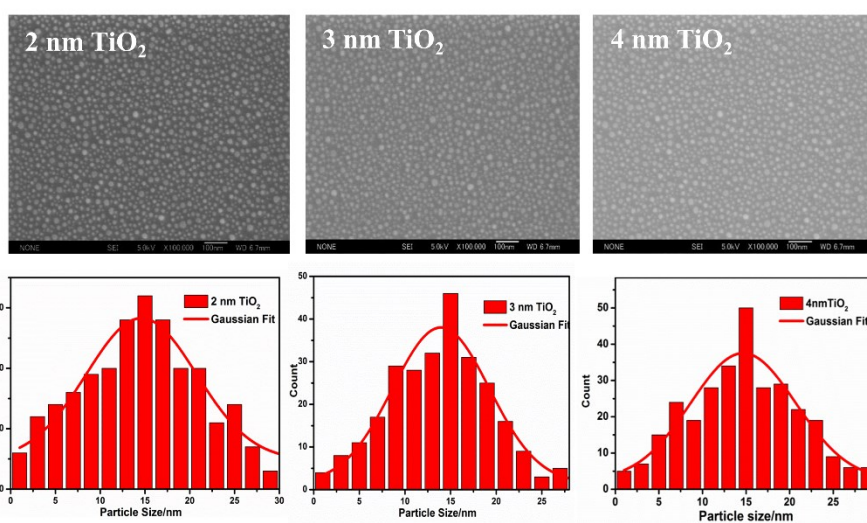


**Fig. S7** Top-view SEM images (upper) and the particle size distributions (lower) of x-nm-TiO<sub>2</sub>/Au-NPs/Ga<sub>2</sub>O<sub>3</sub> (x=2-4).



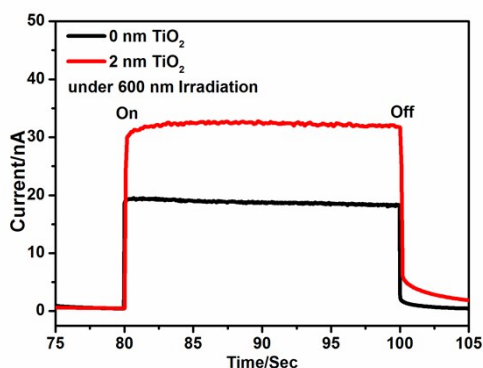


**Fig. S8** *I-t* characteristics Au-NPs/Ga<sub>2</sub>O<sub>3</sub> with 0 and 2 nm TiO<sub>2</sub> under 600 nm irradiation.

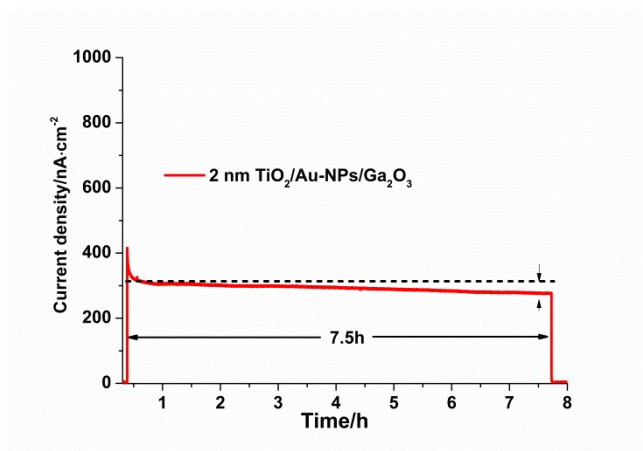


**Fig. S9** Current density-time curve of 2-nm-TiO<sub>2</sub>/Au-NPs/Ga<sub>2</sub>O<sub>3</sub> under 600 nm light irradiation. The measurement conditions were identical to the photocurrent measurements in the manuscript. The dash line meant the initial value of quasi-steady current density.

After 3 minutes irradiation, quasi-steady photocurrent density was obtained as 310 nA/cm<sup>2</sup> as shown in Fig. S9. The photocurrent density after 7.5 hours was 280 nA/cm<sup>2</sup> which showed long-time stability.

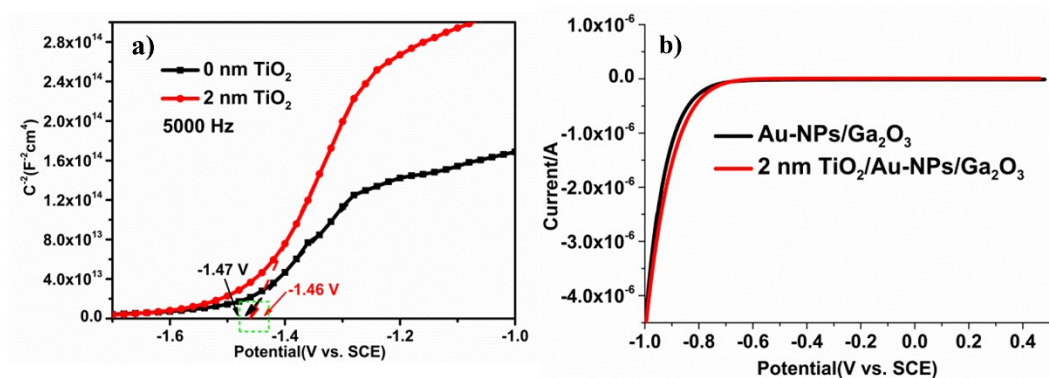


**Fig. S10** (a) A typical Mott–Schottky plot of Au-NPs/Ga<sub>2</sub>O<sub>3</sub> without TiO<sub>2</sub> modification. (b) *I*-*V* characteristics of 2-nm-TiO<sub>2</sub> / Au-NPs/Ga<sub>2</sub>O<sub>3</sub> and Au-NPs/Ga<sub>2</sub>O<sub>3</sub> measured in dark condition.

According to the Mott-Schottky measurement in Fig. S10a, the flat-band potential of Au-NPs/Ga<sub>2</sub>O<sub>3</sub> is estimated to be -1.47 V (vs. SCE at pH 7). Thus, the flat-band potential of Au-NPs loaded Ga<sub>2</sub>O<sub>3</sub> could be concluded to be -0.81 V (vs. RHE) by the following formula:

$$E(\text{RHE}) = E(\text{SCE}) + 0.244 + 0.059 \times \text{pH}.$$

After the deposition of TiO<sub>2</sub>, the flat-band potential shows a further positive shift to -0.80 V vs. RHE which is consistent with the onset potential shift in *I*-*V* result shown in Fig. S10b. The energy barrier of 2.03 eV is calculated between flat-band potential of 2-nm-TiO<sub>2</sub>/Au-NPs/Ga<sub>2</sub>O<sub>3</sub> and the oxidation potential of water (+1.23 V vs. RHE).

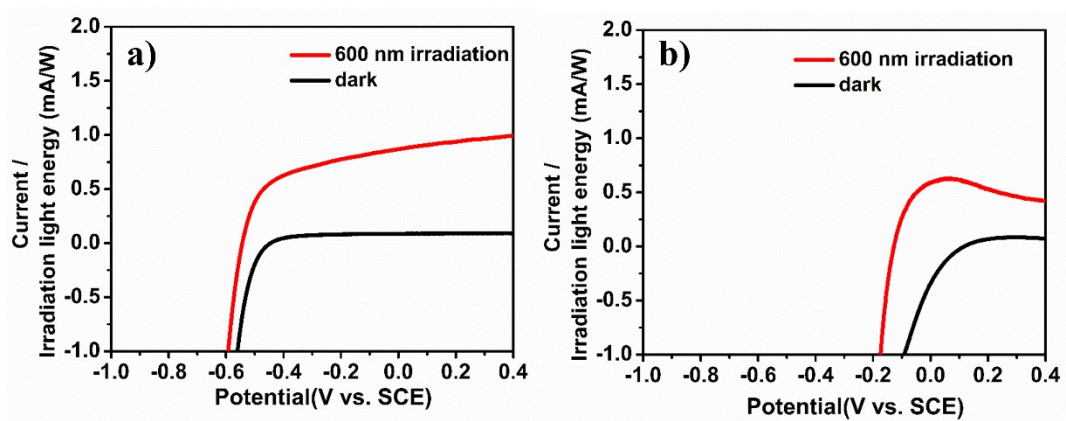


**Fig. S11** *I-V* characteristics of (a) 2-nm-TiO<sub>2</sub>/Au-NPs/Ga<sub>2</sub>O<sub>3</sub> and (b) Au-NPs on TiO<sub>2</sub> thin film with a thickness of 54 nm with and without light irradiation of the wavelength of 600 nm. The current is normalized by the irradiation light energy.

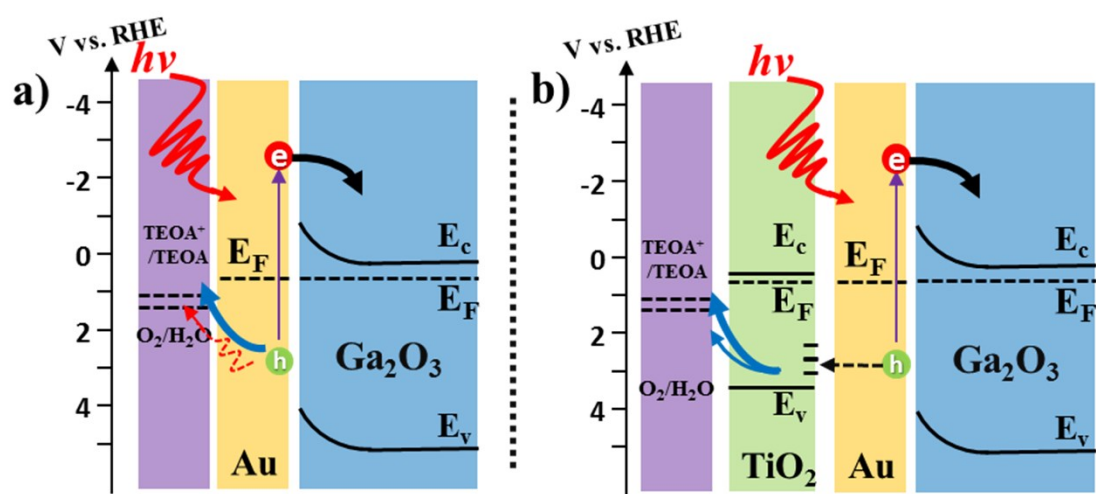


**Fig. S12** Schematics of plasmon-induced charges transfer of (a) Au-NPs/Ga<sub>2</sub>O<sub>3</sub> and (b) 2 nm-TiO<sub>2</sub>/Au-NPs/Ga<sub>2</sub>O<sub>3</sub>. e and h indicate the electrons and holes, respectively.

## Reference

1. W. Mi, X. Du, C. Luan, H. Xiao and J. Ma, *RSC Adv.*, 2014, 4, 30579-30583.
2. B. Bharti, S. Kumar, H. Lee and R. Kumar, *Sci. Rep.* 2016, 6, 32355.